AN ELECTRON SPECTROMETER FOR STUDYING THE AUTOIONIZATION PROCESSES IN METAL VAPORS

A.A. BOROVIK

Institute of Electron Physics, Nat. Acad. of Sci. of Ukraine
(21, Universytets'ka Str., Uzhgorod 88017, Ukraine; e-mail: dep@mail.uzhgorod.ua)

UDC 539.186.188

An electron spectrometer is described for the use in precise studies of the autoionization processes in metal vapors. The spectrometer incorporates both the energy-selected and unselected electron beam sources, a 127° cylindrical deflection electron analyzer and an oven as the source of an atomic beam. The performance of the spectrometer is demonstrated with the measurements of ejected-electron excitation functions for the autoionizing states of sodium and potassium atoms.

1. Introduction

During the last two decades, the autoionization processes in alkali atoms draw the permanent attention of both experimentalists and theoreticians for two main reasons. The first one consists in a unique possibility for studying a wide range of atomic phenomena accompanying both the electron excitation of autoionizing states (e.g., the exchange- and configuration interactions, cascade population, negative-ion resonances) and their subsequent decay (ionization, autoionization, quasimetastability, metastability). The significance of these fundamental data for understanding atomic spectroscopy cannot be overestimated. The second reason involves the important role of autoionizing states in the formation of the charge composition, repopulating and energy transferring processes in the plasma environment of different electric discharges and plasma devices, including EVU-lasers, where the metal vapours are widely used as a basic or additional component [1].

The main peculiarity of experimental studies of autoionization processes in metal atoms by electron spectroscopy is the strong influence of chemically active metal vapors on the performance of analyzing and detecting devices. Such an influence results in uncontrolled changes of the experimental conditions, namely, the energy scales, transmission of electron analyzers, intensity of the incident electron beam, detector efficiency etc. The underestimation of these factors can make the whole measuring procedure unfeasible, especially in case where both the reliable statistics and accuracy of the measured data are sought by the experimentalists. For minimizing the influence of the negative factors mentioned above, some special measures have to be undertaken in the design of main parts of the experimental arrangement, namely, the metal vapor source, input- and output electron optics of analyzers, scattering geometry. At the same time, the objective tests for controlling the experimental conditions have to be developed as well. The additional problems arise in the realization of high-resolution studies of autoionization processes in the near-threshold impact energy region. These are the small excitation cross sections and a low intensity of the energy-selected electron beam.

Since 1997, the INTAS research projects "Collisions of slow electrons with atoms, ions and molecules" (No. 96-0477) and "Dynamics of correlated particles in the continuum" (No. 03-51-4706) were successfully performed at the Department of Electron Processes of the Institute of Electron Physics of NASU. Within the framework of these projects, an electron spectrometer was designed for the precise studies of autoionization processes in metal vapours. Unlike the other known experimental apparatus (see, e.g., [2–6]), it allows the accurate data on the ejected-electron spectra to be obtained both in the near-threshold and in the high impact energy regions. As a result, a number of pioneer studies of the resonance processes in alkali and alkali-earth metals were performed using both energy-selected and unselected electron beams [7–12]. In the present work, we describe this apparatus and show its performance by the example of the recent data on the ejected-electron excitation functions of the autoionizing states in sodium and potassium atoms.

2. Design Principles and Construction

The electron spectrometer consists of a source of incident electrons, an analyzer of scattered electrons, and a source

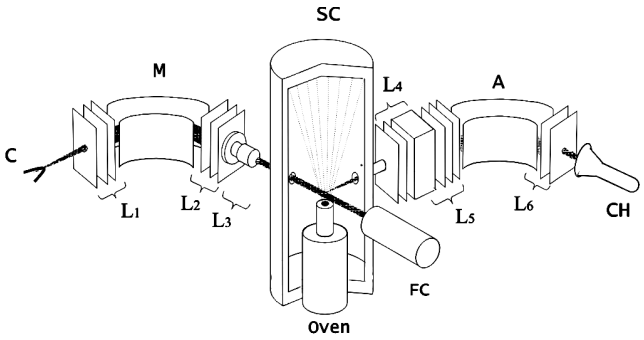

Fig. 1. Ejected-electron spectrometer: C – cathode; M and A – 127° electron monochromator and analyzer, respectively; L_{1-6} – electron-optical lenses; SC – scattering chamber; FC – Faraday cup; CH – channel electron multiplier. The oven is located at 90° to the beam scattering plane. The base flange is not shown

of metal vapours. The relative position of all components of the spectrometer inside the vacuum chamber is shown in Fig. 1. The whole assembly is mounted on a water-cooled base flange. A volume with interacting electron- and atomic beams is surrounded by a copper cylinder (the so-called "scattering chamber") with suitable orifices in the scattering plane that allow the incident beam to enter and to leave the scattering volume and the ejected scattered electrons to reach the electrostatic analyzer. Such a design provided the independent technical service and the fast adjustment of each device in respect to the whole assembly. The top of the scattering chamber is covered by a thick copper cup serving as a water-cooled vapour trap. To provide the effective degassing and to minimize temperature gradients inside the vacuum chamber, all parts of the spectrometer were heated separately by the resistive heaters. The temperature was continuously monitored by several K-type thermocouples. The spectrometer is placed inside a vacuum chamber of $300 \times 300 \times 300$ mm in dimension constructed from nonmagnetic stainless steel Kh18N10T and shielded inside by three layers of permalloy sheets each 1 mm thick. An external resistive heater was used for degassing the chamber at a temperature about 200 °C. The residual pressure of approximately 10^{-7} Torr inside the chamber was provided by the vacuum system contained a backing pump (NVR-16D), a diffusion oil pump (NVD-0, 15) equipped by a water-cooled trap, and an ion pump (NMD-0, 4-1). To minimize an influence of the magnetic field of the ion pump, the latter was attached to the vacuum chamber through a stainless steel pipe of 500 mm in length and 150 mm in width.

The electron spectrometer operates in the following way. The incident electron beam crosses the vapour beam at an angle of 90°. As a result of collisions between the incident electrons and the target atoms, there are two groups of electrons passing the entrance slit of the electron analyzer. The first group consists of the incident electrons elastically or inelastically scattered on atoms providing the so-called electron energy-loss spectrum. The second group consists of the ejected electrons arising from the ionization and autoionization of target atoms. These electrons form an ejected-electron spectrum. Electrons having passed the input electron-optical system of the analyzer are focused at the entrance slit of the 127° electrostatic deflector. Those electrons having passed the deflector are accelerated by an output lens and detected by a channel electron multiplier. Below, we describe the design of the spectrometer in detail, by focusing on the peculiarities concerned with providing the minimal influence of metal vapors on the spectrometer performance.

I n c i d e n t e l e c t r o n b e a m s o u r c e s. The electron beam of regulated energy is widely known as the technically simplest but powerful tool for studying the dynamics of a collision process [13]. Measuring the scattering and ejected-electron spectra or the excitation cross-section for individual atomic levels yields the valuable information about the interaction of an incident electron and a target atom at different impact energy regimes. Moreover, such data provide important tests of theoretical models and stimulate the further development of theoretical approaches. Note, however, that the above advantages can only be fully realized if an incident electron beam with well-defined energy is used. Such a beam can be provided by using the electron energy selectors (monochromators) [14]. The latter are especially effective when the precise data on the excitation dynamics of an atomic process with a sufficiently large efficiency are necessary to be obtained. However, in case of a low efficiency of the excitation process, the reliable data could only be obtained if a specially designed "conventional" electron gun is used in measurements. In the present spectrometer, both a "conventional" electron gun and an electron monochromator were used as the source of incident electrons. In both designs, the cathode was made of a thoriated tungsten wire of 0.15 mm in diameter. Such a cathode retains its emission properties even after the repeated air/metal vapour exposures. The multielement electron lenses were used for the geometric shaping of the electron beam along the sources.

The electron-optical system and the whole construction of a gun are shown in Fig. 2. It was based on our former design [15] essentially modified to fit with the present experimental requirements. The electron-optical system of the gun consists of an immersion two-element lens L_1, a symmetric three-element lens L_2 and an output non-symmetric three-element lens L_3. Such a design provides the output geometry and the intensity of the beam stable in a wide energy region of 30–600 eV. In order to minimize an influence of the space charge formed by the reflection of slow electrons inside the lenses, the latter were of a cylindrical type [16]. For the geometric adjustment of the beam with respect to the scattering volume, the electrostatic deflectors $D_{1,2}$ were placed close to the gun exit.

The electron-optical system of the monochromator is shown in Fig. 1. A short-focus three-element lens L_1 provides the formation of an electron beam with a minimal angular spread and at a fixed pass energy at the entrance of the 127° cylindrical electrostatic deflector which served as a dispersion element. In order to minimize the space charge caused by reflected electrons inside the deflector, the cylinder plates were made of a high-transparency molybdenum grid. The output optical system of the monochromator consists of a short-focus three-element lens L_2 and a long-focus two-element lens L_3. The lenses $L_{1,2}$ are of a slit type, while the lens L_3 is of a cylindrical type. In order to neutralize an influence of the external electromagnetic fields on the performance of the monochromator, the latter was installed in a 0.2-mm-thick Skudotech shield [17]. This substantially improved the energy resolution and transmission at the lowest pass energy of the monochromator.

The incident electrons having passed through the scattering volume were collected by a Faraday cup (see Fig. 1). The latter consists of two cylinders used for monitoring the focusing of the beam at different impact energies. In the energy region of 15–200 eV, an angular spread of the beam did not exceed 5° for both types of electron sources. In order to suppress the secondary electrons which would contribute to the background of the measured electron spectra, the inner cylinder was set to +12 V. The energy spread of the electron beam was measured by observing the peak of elastically scattered electrons in the residual gas energy loss spectra. Since this peak is a result of the convolution of the analyzer apparatus function and the energy distribution function of the electron beam, one should consider its width as an upper value of the actual energy spread of the beam. Figure 3,*a, b* shows the current-to-voltage characteristic

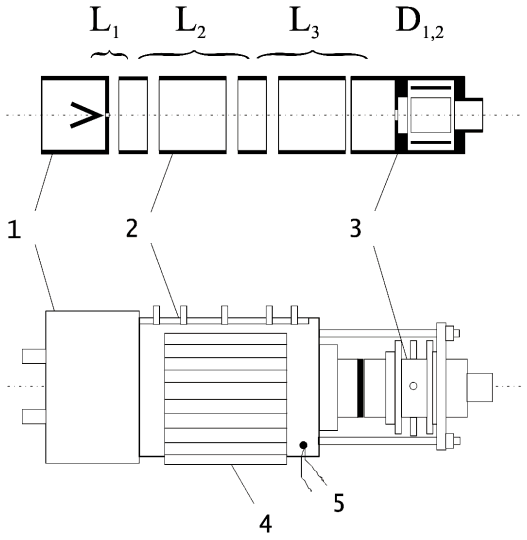

Fig. 2. Schematic diagram of the electron-optical systems and the design of the electron gun: *1* – cathode unit; *2* – electrodes of electron-optical lenses $L_1 - L_3$; *3* – beam deflectors $D_{1,2}$; *4* – heater; *5* – thermocouple

and the typical energy spread of the output electron beam for the gun and the monochromator, respectively.

E l e c t r o n e n e r g y a n a l y z e r. The electron energy analyzer used in the present work was similar to that designed earlier for the threshold electron spectroscopy purposes [18], however, a modification of the input lens system was made to adjust its focusing properties to the present scattering geometry. The whole electron optical system is shown in Fig. 1. Since the energies of analyzed electrons in the present work were expected to be between 5 and 50 eV, the maximum transmission of the input electron optics was provided by addition of a double-element lens L_4 placed just after the entrance slit. A double-element lens L_6 provided the acceleration and the focusing of electrons at the input of the channel electron multiplier VEU-6. In order to prevent an influence of external electrical fields and metal vapors, the analyzer was thoroughly screened by a non-magnetic shield. Two resistive antiinductively wound heaters placed close to the input and the middle of the analyzer provided its permanent heating at temperatures up to 100 °C. The analyzer was positioned at an observation angle of 54.7°. In this case, the detected ejected-electron intensity does not depend on the alignment of the autoionizing states [19]. During the measurements, the typical energy and the angular resolution of the analyzer were 0.15 eV and ±3.2°, respectively.

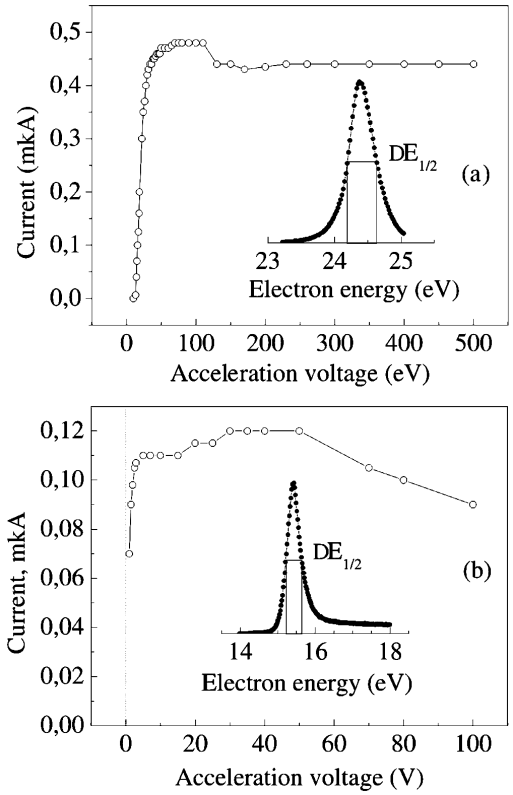

Fig. 3. Current-to-voltage characteristics and energy spread of incident electron beams for the gun (*a*) and monochromator (*b*)

A t o m i c b e a m s o u r c e. The atomic beam source was designed by taking the following requirements into consideration:

– it should provide a stable well-collimated beam of atoms of metals with evaporation temperatures up to 600 °C;

– its magnetic field should not affect the collision region;

– its run time at a vapor density in the collision region 10^{12} atoms/cm^3 should not be less than 48 h.

The present apparatus was equipped with a resistively heated, antiinductively wound oven shown schematically in Fig. 1. Its whole design is similar to that described earlier in [20]. However, the distinct feature of the present oven is the 30-mm-long and 3-mm-wide vapor transportation channel which allowed both the atomic beam maximally to approach the collision center and to move the magnetic field of a heater off the scattering area. In order to minimize the vapour flow, the atomic beam was formed by a 10-mm-long and 1-mm-wide nozzle mounted at the output end of a crucible. In order to avoid the blockage of the nozzle, its temperature was kept approximately by 50 °C higher than that of the bottom of the crucible. The latter was electrically insulated from the oven body by a teflon ring. The focusing of the electron beam at low incident energies was controlled by measuring the current of electrons which hit the nozzle. To minimize the heat losses, both the crucible and the heather were enclosed in a stainless steel shield and then in a copper water-cooled jacket which served also as the bottom part of the scattering chamber (see Fig. 1). The oven was tested in the measurements with lithium vapors at temperatures up to 600 °C [7, 21]. It is worth to note that the main design principles of the present source were successfully used recently in designing a magnesium beam source [22].

D a t a a c q u i s i t i o n e l e c t r o n i c s a n d m e a s u r i n g p r o c e d u r e. The main goal of the present experimental arrangement consisted in systematic studies of electron spectra at the impact energies close to the energy threshold of a core-excitation process. Due to the extremely low detecting signal, such measurements require the efficient data acquisition system and the thorough control of experimental conditions. The data acquisition system designed for the present electron spectrometer is shown in Fig. 4. During the measurements, a personal computer via a specially developed software varies the incident beam energy, scans the energy of scattered and ejected electrons, sets the dwell time of the measurements by monitoring the current of the incident beam, and stores the analyzer output signal. In order to minimize the background level in the detecting signal, the specially designed low-noise power supplies and thoroughly screened electrical junctions were used in the spectrometer.

The whole experimental procedure, including the energy scales calibration, the control of experimental conditions, and processing the data, was described in details elsewhere [7, 8]. Briefly, the ejected-electron spectra were measured step-by-step at different values of the incident electron energy. The spectra were automatically normalized to the intensity of the incident electron beam by a "current-to-frequency" converter. To control the stability of the experimental conditions during the entire measurement, a "test" spectrum at a fixed impact energy was measured before and after each set of five ejected-electron spectra. For obtaining the excitation functions for the particular autoionizing states, the sets of spectra were processed for subtracting the intensity of the background and for deriving the line intensities by using the ORIGIN software package.

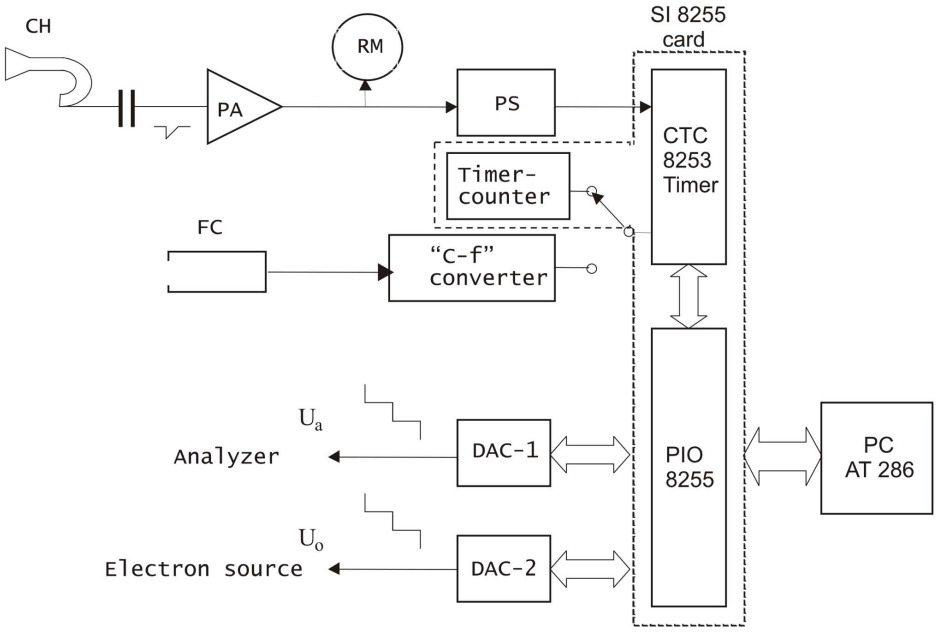

Fig. 4. Block diagram showing the data acquisition electronics: *CH* – channel electron multiplier; *PA* – pre-amplifier; *RM* – rate meter; *PS* – pulse shaper; *FC* – Faraday cup; *DAC-1, 2* – digital-to-analog converters

3. Performance of the Spectrometer

By using the experimental arrangement described above, the ejected-electron spectra of sodium and potassium atoms were obtained for the first time at the incident electron impact energies close to the excitation threshold of the $np^5n_1\ell_1n_2\ell_2$ autoionizing states ($n = 2$, 3 for sodium and potassium, respectively). These data were used to obtain the accurate excitation functions of the lowest $np^5(n+1)s^2$ autoionizing states in these atoms.

S o d i u m. The ejected-electron spectra of sodium atoms in the region of the $(2p^53s^2)^2P_J$ states are shown in Fig. 5,*a*. As can be seen, the present ejected-electron energy resolution of 0.1 eV was insufficient to avoid some overlapping of the $^2P_{3/2}$ and $^2P_{1/2}$ lines. Such a situation might result in an additional uncertainty in the determination of line intensities, especially, in the near-threshold impact energy regime, where the energy position and the shape of lines could be affected by the post-collision interaction (PCI) [23].

However, the rough estimate using the calculated lifetimes for the $^2P_{3/2}$ and $^2P_{1/2}$ states [24] limits an influence of the PCI effect to 10% or less. In the whole 30–75 eV impact energy region under study, no additional structure was observed in the spectra close to the $^2P_{3/2}$ and $^2P_{1/2}$ lines.

Figure 5,*b* presents the ejected-electron excitation functions for the $(2p^53s^2)^2P_{3/2}$ and $^2P_{1/2}$ autoionizing

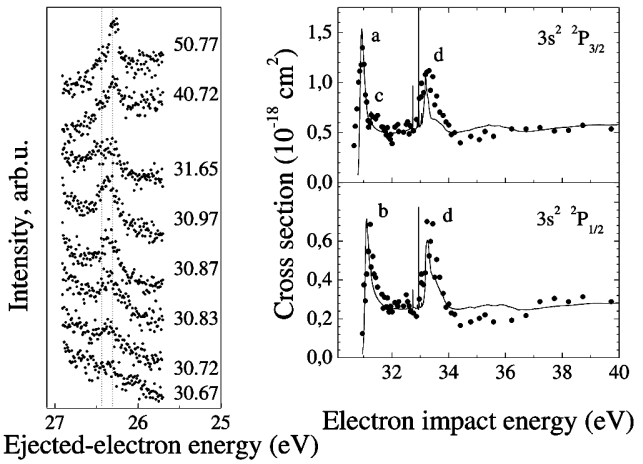

a **b**

Fig. 5. Ejected-electron spectra (*a*) and excitation functions (*b*) for the $2p^53s^2$ autoionizing states of sodium atoms measured at near-threshold impact energies. In Fig. 5, *b*, dots mark the experimental results, whereas solid lines present the *R*-matrix calculations [25]

levels in sodium in the impact energy range from the corresponding excitation thresholds up to 40 eV and the calculated angle-integrated cross sections obtained in the *R*-matrix (close-coupling) approach [25]. The relative experimental data were put on an absolute scale by normalizing visually the $(2p^53s^2)^2P_{3/2}$ excitation function to the theoretical results obtained in the

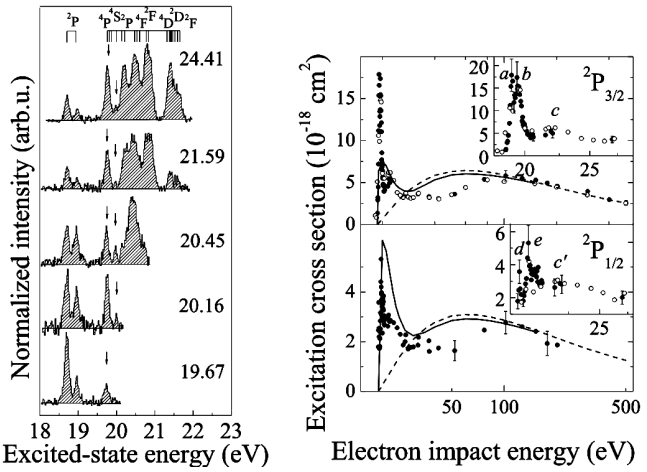

a b

Fig. 6. Same as in Fig. 5 except the data are for the $3p^5 4s^2$ autoionizing states of potassium atoms. In Fig. 6,*b*, solid and open circles mark the present and former [6] experimental data, whereas solid and dashed lines present the results of DWBA and PWBA calculations, respectively [8]

nonresonant regime above the 34-eV incident energy. In the near-threshold energy region, both the functions exhibit similar shapes characterized by two prominent features labelled *a* and *d* for the $^2P_{3/2}$ state and *b* and *d* for the $^2P_{1/2}$ state. Due to the improved energy resolution of the present measurements, this is the first time that the resonance features *a*–*d* are revealed in both excitation functions individually. The resonances exhibit remarkably asymmetric shapes characterized by a slower decrease of the cross section at the side of higher impact energies. The main differences between the two functions lie in the relative intensities of the resonances and in the presence of a weak feature *c* in the excitation of the $^2P_{3/2}$ level.

Comparing the experimental and calculated cross sections for the $(2p^5 3s^2)^2 P_{3/2,1/2}$ levels presented in Fig. 5,*b*, it is worth noting a good agreement between the theory and experiment regarding the sharp rise of the excitation cross section just above the respective thresholds, as well as in the broad feature between 33 and 34 eV. In order to show the narrowness of some of the features, the theoretical results are depicted without convolution with the experimental energy resolution. The analysis of the theoretical data shows that the features *a*–*d* reflect the presence of strong negative-ion resonances with likely configurations $2p^5 3s^2 3p$ and $2p^5 3s 3p^2$ close to the excitation threshold of the $(2p^5 3s^2)^2 P_{3/2,1/2}$ states.

P o t a s s i u m. Figure 6,*a* shows the ejected-electron spectra of potassium atoms in the region of the lowest autoionizing states of the $3p^5 4s^2$, $3p^5 4s4p$, $3p^5 3d5s$, and $3p^5 4s5s$ configurations. A notable peculiarity of these spectra is a remarkable high intensity of lines at the threshold impact energies. Thus, in the spectrum at 19.67 eV, the ^4P line intensity is 1/3 of its maximum value observed at 21.1 eV. In the spectrum at 20.45 eV, the group of lines with thresholds around 20.5 eV has the intensity of approximately 2/3 of the maximum value. Such a resonance behavior of the excitation of above levels explains an abrupt increase of the total autoionization cross-section observed earlier at the 20.45-eV impact energy [9].

The ejected-electron excitation functions for the $(3p^5 4s^2)^2 P_{3/2}$ and $^2P_{1/2}$ autoionizing states are shown in Fig. 6,*b* together with the theoretical data obtained in the plane-wave Born (PWBA) and in the distorted-wave Born (DWBA) approximations [8]. The relative experimental data were put on the absolute scale by normalizing the $(3p^5 4s^2)^2 P_{3/2}$ excitation function to the PWBA cross-section at 500 eV [26].

For the impact energies above 20 eV, the general shape of the excitation functions in the present measurements is very similar to that for the data obtained earlier in [26]. A difference can be seen for the $^2P_{3/2}$ level close to 22 eV and 100 eV, where the cross sections differ by approximately 15%, but this is still within the error bars. For the incident energies between 30 and 37 eV, both experimental results exhibit the scatter in the data for the $^2P_{1/2}$ level. This is due to the effect of overlapping the ejected-electron spectra with associated $3p^5 n_1\ell_1 n_2\ell_2$ energy-loss spectra.

Due to the improved energy resolution of the present measurements, we believe this is the first time that the resonance features *a, b* and *d, e* are revealed in both excitation functions individually. The widths of features *a, d* and *e* do not exceed the experimental resolution, and hence we classify them as the separate resonances. In contrast, a broad asymmetric shape of feature *b* suggests the combined effect of several overlapping resonances. The latter also determines the scatter in the data around 20 eV for the $^2P_{1/2}$ level. Features *c* and *c′* coincide in energy and are similar in shape. As seen from the comparison with other data [26], their observed widths do not depend significantly on the energy resolution. The resonance parts of the total excitation cross-section for the $^2P_{3/2}$ and $^2P_{1/2}$ levels reach their respective maximum values of 17.9×10^{-18} cm^2 at 19.12 eV (feature *a*) and 5.3×10^{-18} cm^2 at 19.66 eV (feature *e*). Note that

these values exceed substantially the cross sections in the broad maxima around 100 eV. The observed resonances were classified with the $3p^5 3d4s^2$ negative-ion configuration on the base of the R-matrix (close-coupling) calculations [8].

In addition to the data on resonances, the cascade radiative transitions between the fast decaying autoionizing doublet states were also revealed for the first time in sodium [27] and potassium [10]. These results have changed the former prevailing view on the low efficiency of such transitions due to the fast Coulomb autoionization of the upper (cascading) levels. As it was clearly shown, the observed high efficiency of radiative cascades is caused by the strong resonance excitation of the high-lying autoionizing states.

This work was supported by the INTAS Research Projects No.96-0477 and No.03-51-4706.

1. *Laser Techniques in the Extreme Ultraviolet*, edited by S.E. Harris and T.B. Lucatorto (AIP, New York, 1984).
2. A.A. Borovik, H. Rojas, G.C. King, and E.Yu. Remeta, J. Phys. B **32**, 4225 (1999).
3. O.O. Borovik, V.M. Krasilinec, and I.S. Aleksakhin, Ukr. Fiz Zh. **42**, 400 (1996).
4. A.J. Murray and P. Hammond, Rev. Sci. Instrum. **70**, 1939 (1999).
5. D. Cvejanovic and A.J. Murray, Meas. Sci. Technol. **13**, 1482 (2002).
6. B. Feuerstein, A. Grum-Grzhimailo, and W. Mehlhorn, J. Phys. B **31**, 593 (1998).
7. A.A. Borovik and V.N. Krasilinec, J. Phys. B **32**, 1941 (1999).
8. A.A. Borovik, A.N. Grum-Grzhimailo, K. Bartschat, and O. Zatsarinny, J. Phys. B **38**, 1081 (2005).
9. M.J. Evrij, A.A. Borovik (jr.), L.L. Shimon *et al.*, Nucl. Instr. Meth. B **233**, 280 (2005).
10. A. Kupliauskiene, P. Bogdanovich, A. Borovik *et al.*, J. Phys. B **39**, 591 (2006).
11. A.A. Borovik (jr.), A.A. Borovik, O.I. Zatsarinny, and K. Bartschat, Phys. Rev. A **73**, 062701 (2006).
12. A.A. Borovik, V.V. Vakula, and A. Kupliauskiene, Lith. J. Phys. **47**, 129 (2007).
13. S.J. Buckman and C.W. Clark, Rev. Mod. Phys. **66**, 539 (1994).
14. J.B. Hasted, Contemp. Phys. **14**, 357 (1972).
15. A.A. Borovik, Sov. Phys. IET A **3**, 124 (1991).
16. D.W.O. Heddle and M.V. Kurepa, Sci. Instrum. **3**, 552 (1970).
17. http://www.skudotech.com.
18. G.C. King, M. Zubek, P.M. Rutter, and F.H. Read, J. Phys. E **320**, 440 (1987).
19. E.G. Berezko and N.M. Kabachnik, J. Phys. B **10**, 2467 (1977).
20. A. Borovik, H. Rojas, and G.C. King, Meas. Sci. Technol. **6**, 334 (1995).
21. A.A. Borovik and V.V. Skubenich, *Abstracts of Contributed Papers, XXV ICPEAC, Freiburg, Germany, 2007*, Fr092.
22. P. Bolognesi, G. Bogachev, V. Borovik *et al.*, J. Phys. B **41**, 015201 (2007).
23. P. van der Straten, R. Morgenstern, and A. Niehaus, Z. Phys. D **8**, 35 (1988).
24. O.I. Zatsarinny and L.A. Bandurina, J. Phys. B **26**, 3765 (1993).
25. A.A. Borovik, O. Zatsarinny, and K. Bartschat, J. Phys. B **41**, 035206 (2008).
26. B. Feuerstein, A. Grum-Grzhimailo, and W. Mehlhorn, J. Phys. B **32**, 4547 (1999).
27. A. Kupliauskiene, P. Bogdanovich, L. Shimon, and A. Borovik, *Abstracts of Contributed Papers, XXV ICPEAC, Freiburg, Germany, 2007*, Fr063.

Received 04.02.08

ЕЛЕКТРОННИЙ СПЕКТРОМЕТР ДЛЯ ДОСЛІДЖЕНЬ АВТОІОНІЗАЦІЙНИХ ПРОЦЕСІВ В ПАРАХ МЕТАЛІВ

О.О. Боровик

Р е з ю м е

Описано електронний спектрометр для прецизійних досліджень автоіонізаційних процесів у парі металів. Спектрометр містить джерела селективного і неселективного за енергією електронних пучків, 127° циліндричний електронний аналізатор та джерело атомного пучка. Експлуатаційні якості спектрометра продемонстровано на вимірюваннях функцій збудження автоіонізаційних станів атомів натрію та калію.